Title

Novel Strategy for Photopatterning Emissive Polymer Brushes for Organic Light Emitting Diode Applications

Journal

ACS Central Science, 3(6)

ISSN

2374-7943

Authors

Page, Zachariah A
Narupai, Benjaporn
Pester, Christian W
et al.

Publication Date

2017-06-28

DOI

10.1021/acscentsci.7b00165

Peer reviewed

ACS central science

Research Article

http://pubs.acs.org/journal/acscii

Novel Strategy for Photopatterning Emissive Polymer Brushes for Organic Light Emitting Diode Applications

Zachariah A. Page,[†] Benjaporn Narupai,[†,‡] Christian W. Pester,[†] Raghida Bou Zerdan,[†] Anatoliy Sokolov,[§] David S. Laitar,[§] Sukrit Mukhopadhyay,[§] Scott Sprague,[§] Alaina J. McGrath,[†] John W. Kramer,[§] Peter Trefonas,[⊥] and Craig J. Hawker*[,†,‡]

[†]Materials Research Laboratory and [‡]Department of Chemistry and Biochemistry, University of California Santa Barbara, California 93106, United States

[§]The Dow Chemical Company, Midland, Michigan 48674, United States

[⊥]The Dow Electronic Materials Company, 455 Forest Street, Marlborough, Massachusetts 01752, United States

Supporting Information

ABSTRACT: A light-mediated methodology to grow patterned, emissive polymer brushes with micron feature resolution is reported and applied to organic light emitting diode (OLED) displays. Light is used for both initiator functionalization of indium tin oxide and subsequent atom transfer radical polymerization of methacrylate-based fluorescent and phosphorescent iridium monomers. The iridium centers play key roles in photocatalyzing and mediating polymer growth while also emitting light in the final OLED structure. The scope of the presented procedure enables the synthesis of a library of polymers with emissive colors spanning the visible spectrum where the dopant incorporation, position of brush growth, and brush thickness are readily controlled. The chain-ends of the polymer brushes remain intact, affording subsequent chain extension and formation of well-defined diblock architectures. This high level of structure and function control allows for the facile preparation of random ternary copolymers and red−green−blue arrays to yield white emission.

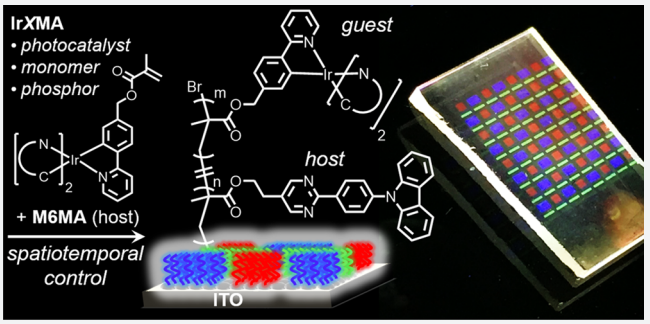

INTRODUCTION

Organic light emitting diode (OLED) displays are among the most energy-efficient two-dimensional display technologies and can be found in everyday appliances, including smartphones, laptops, and televisions.[1,2] However, the efficiency of OLED displays is offset by the cost of production, in part, due to the use of evaporative deposition processes.[3,4] While solution-based methods are attractive alternatives that grant access to low-cost, large area, and high throughput fabrication (e.g., spin-coating, roll-to-roll, etc.), these approaches inherently suffer from limited patterning capabilities. A major challenge is the development of a simple method to generate phosphorescent OLED arrays using solution-based processes.

Display technology often relies on the use of white light to render colored images. Traditionally, white light is obtained by blending red, green, and blue (RGB) emission, which, through clever engineering, can be achieved using a variety of device architectures and pixel layouts.[5−10] Although a number of methods to achieve emissive patterned OLED arrays from solution have been developed, practical limitations such as fabrication complexity, singlet-only emission, scalability issues, low feature resolution, and the use of undesirable reagents have prevented commercialization.[11−15] For example, printing and lithographic techniques require either complex equipment or numerous iterative processing steps,[11−14] while photo-cross-linking is more rapid, but utilizes intense ultraviolet (UV) radiation and photoinitiators[15−19] that contaminate the emissive layer (EML) in an OLED device.

State-of-the-art solution-based patterning procedures achieve spatial resolution either by physically separating the emissive materials during deposition (printing/lithography) or by UV-cross-linking. For the latter approach, the irradiated area is rendered insoluble, which, after washing away un-cross-linked material, allows for subsequent deposition. In contrast to these multistep procedures, surface-initiated growth of polymer brushes has been used for nonpatterned semiconducting[20−23] and patterned insulating polymers[24−29] with a variety of external stimuli being used to provide spatial control.[30,31] In particular, surface initiated atom transfer radical polymerization (SI-ATRP) catalyzed by photoactive Ir(III) phosphors can be used to pattern polymer brushes using visible light,[32] and the "living" nature of this process permits hierarchical patterning of block copolymer brush architectures with submicron feature resolution.[26]

Received: April 16, 2017
Published: June 7, 2017

DOI: 10.1021/acscentsci.7b00165
ACS Cent. Sci. 2017, 3, 654−661

Scheme 1. General Route to Graft Emissive Polymer Brushes from ITO[a]

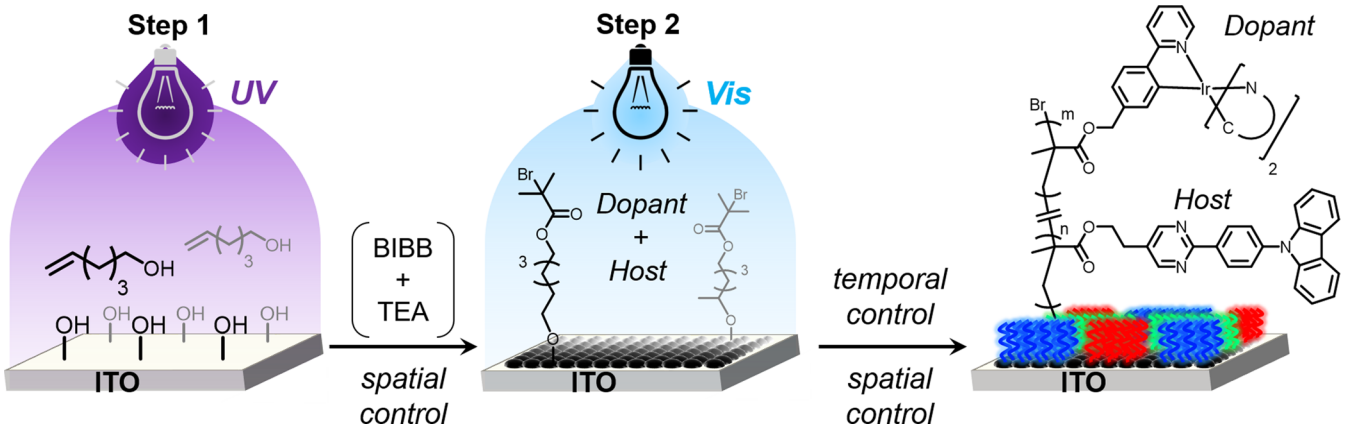

[a]Step 1: functionalization of ITO with 5-hexenol using UV light followed by acylation with α-bromoisobutyryl bromide (BIBB). Step 2: growth of electronically active polymer brushes with visible light.

Significantly, Ir(III) complexes are also widely used as dopants in semiconducting host matrices for OLED devices based on high photoluminescence quantum yield (PLQY), stability, short triplet (T_1) state lifetimes, and spectral tunability from blue to near-infrared.[33−35] In addition, covalent attachment of the Ir(III) complexes to the host mitigates phase separation to further improve device longevity.[36−38]

Here we introduce novel Ir(III) photocatalysts to grow patterned, electronically active, polymer brushes from indium tin oxide (ITO) substrates (Scheme 1). Notably, the Ir(III) species initially acts as a photocatalyst to initiate/mediate polymerization of the brush architectures and then as a covalently bound phosphorescent dopant for patterned OLED devices with a carbazole-based host.[39] Spatiotemporal control, color mixing through copolymerization, chain extension to diblock polymer brushes, and white emission from a red, green, blue pixel array are demonstrated using this novel methodology. As a final demonstration, functional multicolored OLEDs are fabricated to highlight the utility of these materials in next generation display technologies.

RESULTS AND DISCUSSION

The host repeat unit, termed **M6MA**, was selected to be a carbazole-phenyl-pyrimidine moiety covalently attached to a polymerizable methacrylate group. **M6MA**, shown in Scheme 2a, was conveniently prepared in four steps from commercial starting materials.[39] To fully address the potential of white light generation, a library of dopant comonomers with emission spanning the visible spectrum, in particular RGB, were prepared, as shown in Scheme 2b. The heteroleptic and functional Ir(III) complexes were synthesized following initial Nonoyama chemistry[40] to prepare the μ-dichloro bridged dimer (**1**), reaction with silver triflate (AgOTf), and coupling with 4-(pyridine-2-yl)benzaldehyde to yield a range of aldehyde derivatives, **2**. Reduction of **2** provides the corresponding hydroxymethyl derivatives (**3**), followed by acylation with methacryloyl chloride to provide the desired iridium monomers, **IrXMA**, where the C^N ligand, **X**, dictates the triplet (T_1) energy and thus emission color. Specifically, **X** represents difluorophenylpyridine (dfppy), phenylpyridine (ppy), phenylquinoline (pq), or benzothiophenylpyridine (btp) (Scheme 2). Copolymerizations of **M6MA** and **IrXMA** under standard radical conditions confirmed monomer compatibility and allowed for

Scheme 2. Chemical Structures for (a) M6MA and (b) IrXMA Monomers[a]

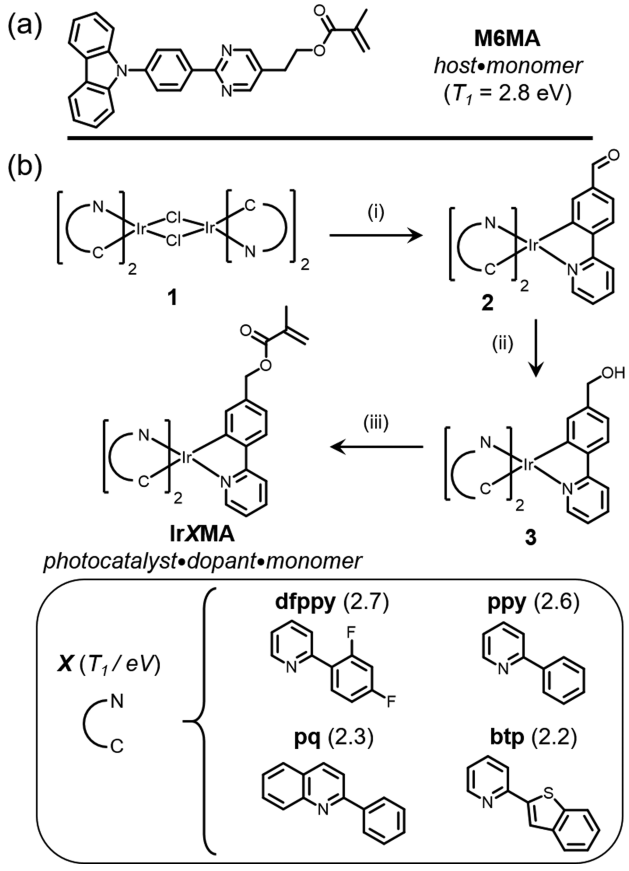

[a]Synthesis of IrXMA, reagents and conditions: (i) AgOTf, 4-(2-pyridyl)benzaldehyde, DMA, 130 °C, 30%. (ii) $NaBH_4$, DCM/EtOH, rt, > 90%. (iii) Methacryloyl chloride, DCM, 0 °C → rt, > 90%. Ligands, their acronyms, and experimental triplet energies provided (bottom).

basic photophysical characterization of the resultant soluble polymers. The copolymers were found to have unique emission profiles dictated by the **IrXMA** comonomer, granting access to turquoise (dfppy), green (ppy), orange (pq), and red (btp) phosphorescence, while homopolymers of **M6MA** provide deep

DOI: 10.1021/acscentsci.7b00165
ACS Cent. Sci. 2017, 3, 654−661

blue fluorescence. It should be noted that the high photoluminescence quantum yield (PLQY ≈ 30−70%) values for the copolymers suggests random monomer incorporation, which mitigates radiative quenching pathways (Table S2).

After establishing monomer compatibility under radical polymerization conditions and examination of the photophysics of the resultant soluble copolymers, an analogous "grafting-from" procedure for polymer brush formation was investigated. Because of its established utility as a transparent electrode in optoelectronic applications, ITO was chosen as the substrate for SI-ATRP. While ITO can be functionalized with silanes and phosphonic acids, these reactions are nonselective.[41] As a result, a photochemical strategy involving the radical coupling with alkenes was chosen, which also provides spatial control.[42,43] Irradiation of ITO with 254 nm UV light in the presence of 5-hexenol followed by acylation of the alcohol functionalized ITO with α-bromoisobutyryl bromide (BIBB) provides initiation sites covalently attached to the surface (Scheme 1, step 1).[44] Surface functionalization was confirmed through X-ray photoelectron spectroscopy (XPS), revealing both bromine and carbonyl functionalities (Figure S11).

Initially, **M6MA** homopolymer brushes were grafted from the initiator-functionalized ITO, using small amounts of $Ir(ppy)_3$ (0.005 mol %) photocatalyst and visible light. The resulting brushes emitted a bright blue fluorescence under UV excitation, characteristic of poly(**M6MA**) thin films measured in our previous study.[39] Since larger quantities of Ir(III) are typically incorporated into the emissive layer of efficient OLEDs, substituting the $Ir(ppy)_3$ photocatalyst with a higher mol % of the **IrXMA** comonomer (1−12 mol %) was considered to be a facile replacement. Indeed, the use of visible light to grow the copolymers provides a library of ITO-tethered brushes having turquoise, green, orange, and red phosphorescence directly matching the analogous soluble polymer samples (Figures 1 and S7). The use of unfunctionalized ITO under the same reaction conditions confirmed that nonspecific polymer adsorption does not occur. The utility of larger quantites of photocatalyst, as is the case for copolymerizations with **IrXMA**, had the added benefit of reducing the amount of light required to elicit brush growth by 1−2 orders of magnitude compared with analogous homopolymer brush growth (Figure S12).[45] Photoluminescence profiles of copolymer brushes (3 mol % **IrXMA**) reveal peak emission wavelengths ranging from 490 to 600 nm with little-to-no residual blue fluorescence from the host, indicative of efficient energy transfer to the Ir(III) dopants. This efficient energy transfer is attributed to the high triplet energy (T_1) of the **M6MA** host ($T_1 \approx 2.8$ eV),[39] relative to the **IrXMA** dopants ($T_1 \lesssim 2.7$ eV) (Tables S1 and S2). XPS was then used to confirm the chemical composition for the five different brushes, with distinct peaks for all brushes. For example, F 1s signals were only observed for poly(**M6MA**-*co*-**IrdfppyMA**) brushes as expected (Figure S13). In addition, indium and tin signals were below detection limits, suggesting uniform coverage with thicknesses exceeding ∼10 nm.

Control of Ir(III) incorporation (i.e., host:dopant ratio) in the emissive layer is critical to overall OLED device performance. To test whether dopant incorporation could be controlled, five different copolymer brushes were grown uniformly on ITO using variable amounts of **IrppyMA** (0, 1, 3, 6, and 12 mol %). XPS was used to determine the chemical composition of the resulting brushes, showing a clear increase in the Ir $4f_{7/2}$ and Ir $4f_{5/2}$ signals at binding energies of 60 and 63 eV, respectively, as the **IrppyMA** loading was increased (Figure 2). Notably, the atomic percent of

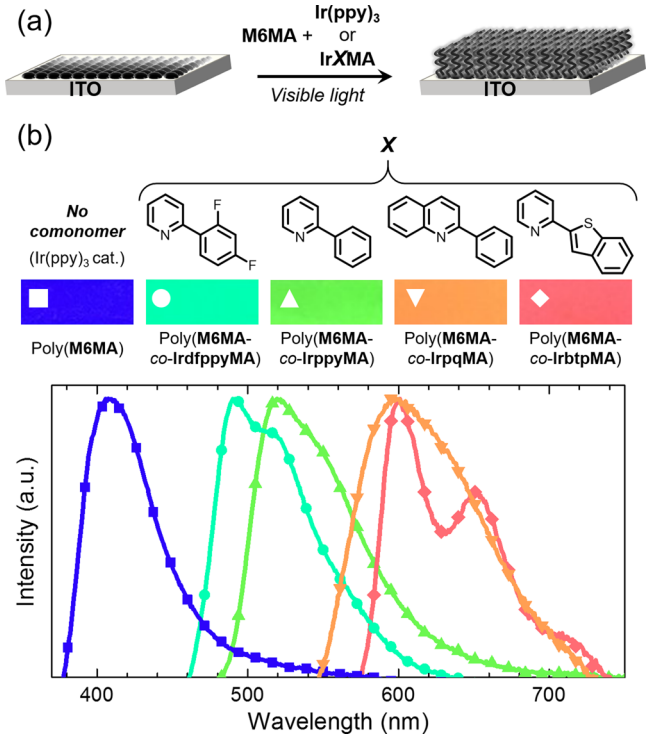

Figure 1. Polymer brushes grafted from ITO using $Ir(ppy)_3$ (0.005 mol %) as the photocatalyst for poly(**M6MA**) and 3 mol % **IrXMA** for copolymers. (a) Schematic representation of grafting from procedure; initiator functionalized ITO to polymer brushes. (b) Chemical structures for C^N ligands (**X**) of **IrXMA** and corresponding photoluminescence profiles. Rectangles are images of the polymer brushes on ITO under 365 nm excitation (Figure S14 for full images).

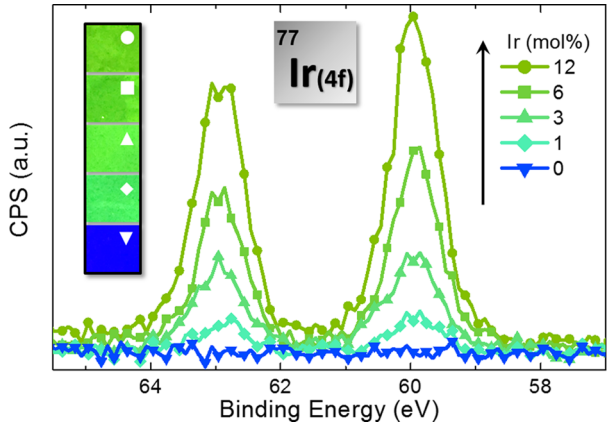

Figure 2. XPS overlay of poly(**M6MA**-*co*-**IrppyMA**) brushes with varied Ir dopant content showing high resolution Ir $4f_{7/2}$ and Ir $4f_{5/2}$ signals at 60 and 63 eV, respectively. Photoluminescence images of the corresponding brushes under 365 nm excitation are provided as an inset.

Ir, relative to carbon, oxygen, and nitrogen, was in good agreement with the expected values (Figure S15). Additionally, photoluminescence measurements on the four copolymer samples reveal a bathochromic shift and broadening of emission for higher **IrppyMA** loadings, which can be observed in the photoluminescence images provided as an inset in Figure 2, and more clearly in the emission profiles given in Figure S16. The noted red-shift and broadening upon increasing dopant content is consistent with the analogous spun-cast soluble polymer samples,[39] indicating that this methodology allows for polymer

DOI: 10.1021/acscentsci.7b00165
ACS Cent. Sci. 2017, 3, 654−661

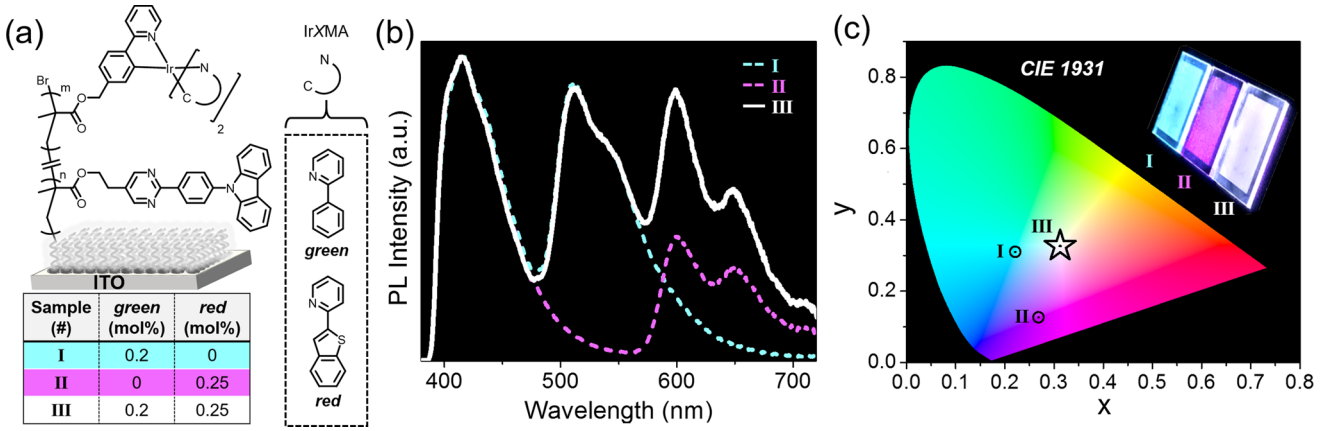

Sample (#)	green (mol%)	red (mol%)
I	0.2	0
II	0	0.25
III	0.2	0.25

Figure 3. White emission from copolymer brushes on ITO. (a) Chemical structures and composition for **I**, poly(**M6MA**-*co*-**IrppyMA**), **II**, poly(**M6MA**-*co*-**IrbtpMA**), and **III** poly(**M6MA**-*co*-**IrppyMA**-*co*-**IrbtpMA**). (b) Photoluminescence profiles showing contributions from red, green, and blue emission for the different copolymer brushes. (c) CIE 1931 coordinates for **I** $(x, y) = (0.22, 0.31)$, **II** $(x, y) = (0.27, 0.13)$, and **III** $(x, y) = (0.31, 0.33)$. Inset is a digital image of the polymer brushes under 365 nm excitation.

brushes with specific dopant content and tunable optical performance to be easily fabricated.

An interesting feature of this copolymer brush strategy is that precise control over dopant concentration makes the generation of white light possible by carefully tuning the composition of red, green, and blue emitting components during random copolymerization (Figure 3a). To demonstrate this ability, we sought to directly obtain white emission by copolymerizing **IrbtpMA** and **IrppyMA** with **M6MA**. In this manner, red and green dopants are copolymerized at low concentration with **M6MA**, allowing for the blue fluorescence from **M6MA** to also be present. Indeed, by carefully tuning the feed ratio of the two **IrXMA** comonomers relative to **M6MA**, white emission was achieved, shown as **sample III** in Figure 3b (Figure S17 for optimization of ternary copolymerizations) with color (x, y) coordinates of (0.31, 0.33) being measured using photoluminescence spectroscopy and matching the white point following 1931 Commission Internationale de L'Éclairage (CIE) guidelines (Figure 3c). It is particularly noteworthy that removing either the red (**I**) or green (**II**) components highlights the respective contribution from each emitter, providing insight into the mechanism of energy transfer within the three component copolymer (**III**) (Figure S18). The difference in peak height for the red emission in **II** and **III** is anticipated, given overlap between the **IrppyMA** emission and **IrbtpMA** absorption, which lends to radiative energy transfer (Figure S18). Visually, there is a dramatic difference between the observable emission colors between **I**, **II**, and **III**, given minute changes in dopant concentrations, as shown in the digital images given as an inset in Figure 3c. This behavior further illustrates the facile emission tunability that is provided with this platform, along with the ability to generate white light for low energy solid-state lighting applications.

For multicolored pixel arrays, the ability to regulate grafting position (e.g., spatial control) is critical and has not been accomplished with electronically active brushes. To investigate this feature, surface patterning using photomasks was examined for either the UV initiator functionalization step (Scheme 1, step 1) or during the visible light-induced polymerization step (Scheme 1, step 2). A chrome coated quartz photomask with transparent rectangular windows (Figure S3, mask 1) was utilized for spatially resolving both light-driven surface chemistries (Figure 4a,b). Significantly, the resulting brushes were spatially resolved in both cases with a notable difference in color for the two reflectance images shown in Figure 4, likely arising from differences in brush height. To further compare both methods, a cross-sectional average of the emission intensity was measured and revealed improved uniformity when employing the photomask during the polymerization process (step 2). Given the superior spatial control achieved during polymer brush growth, this approach was used for all subsequent studies. Moreover, this methodology can be used to provide polymer brush patterns with resolution down to the micron level (Figures 4c and S19), outcompeting state-of-the-art pixels achieved via evaporative deposition ($\sim 5 \times 5\ \mu m^2$).[2,46] These small feature sizes are of particular interest for microdisplay applications, where decreasing pixel dimensions are required to enhance image resolution.[18,47−49]

Since the thickness of each layer in an OLED stack is critical to performance, brush thickness versus time was investigated by patterning poly(**M6MA**) brushes that were grown for different lengths of time followed by analysis with atomic force microscopy (AFM) (details given in the Supporting Information). In Figure 5a the boxed regions are reflectance images, with their center denoted by a cross that corresponds to the specific thickness on the axis, while a 2-point color gradient in between each boxed region was generated from the respective L*,a*,b* color space values as a representation of the theoretical color for any given thickness (Table S4). The distinct color variations for small changes in brush thickness allows for rapid determination of brush height by simply observing the color of reflected white light. In addition, from these results emerged clear evidence for temporal control and direct correlation between polymerization time and brush thickness (Figure S23). To test whether phosphorescent brushes could be grown with temporal control, 6 mol % **IrppyMA** was copolymerized with **M6MA**. The color from reflectance imaging suggests that brush thickness increases with irradiation time, which was further confirmed using AFM of scratched films (Figure 5b). Moreover, the increase in observable emission intensity over time correlates with an increase in brush thickness (Figure 5 inset, bottom). This ability to control copolymer brush formation using only an Ir-functionalized comonomer is significant and illustrates that the generation of phosphorescent pixels of any color on the order of microns in the x, y dimensions and nanometers in the z dimension is possible using this approach.

DOI: 10.1021/acscentsci.7b00165
ACS Cent. Sci. 2017, 3, 654−661

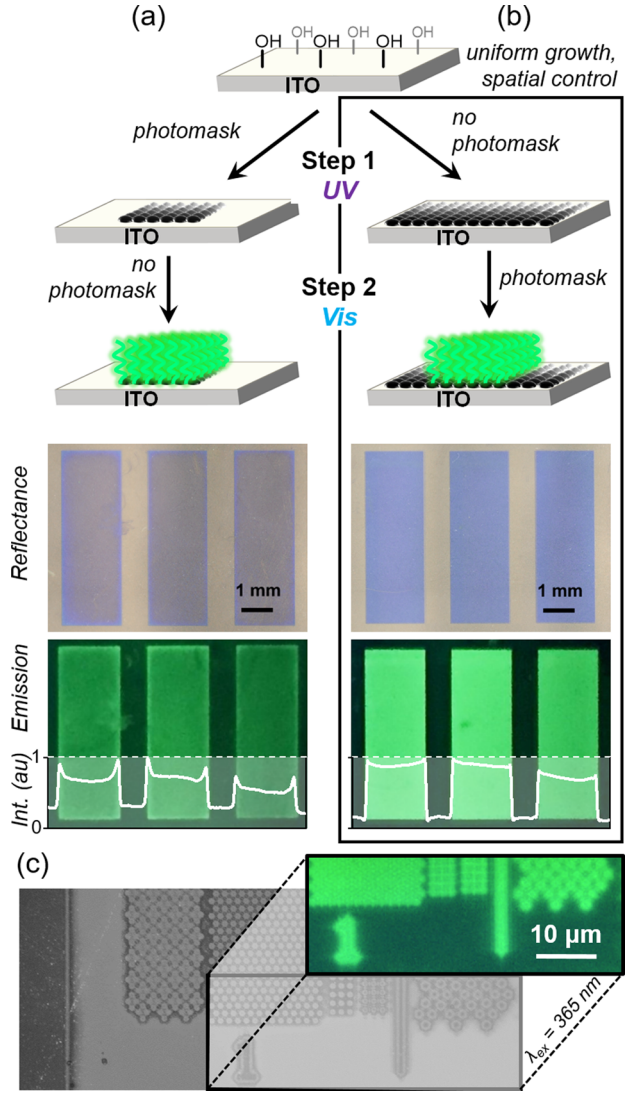

Figure 4. Spatial control for poly(**M6MA**-*co*-**IrppyMA**) brushes containing ∼6 mol % **IrppyMA**, after irradiation through a chrome coated quartz photomask at either (a) step 1 (UV) or (b) step 2 (vis). Schematic representation of the functionalization (top) and corresponding reflectance and photoluminescence images. The inset represents normalized emission intensity as a cross-sectional average, showing improved uniformity and spatial control when employing the photomask at step 2. (c) Micron feature resolution obtained by photopatterned polymer grafting (step 2), showing microscopy images (grayscale reflectance and photoluminescence inset, λ_{ex} = 365 nm).

The most efficient OLEDs to date are multilayers, including a hole transport layer (HTL), electron blocking layer (EBL), emissive layer (EML), hole blocking layer (HBL), and electron transport layer (ETL), making it a necessity to extrapolate beyond the copolymer brushes generated herein to act as an EML. Advantageously, the surface-bound brushes are robust, allowing for subsequent layer deposition to achieve multilayered architectures. Alternatively, the "living" nature of the controlled photoATRP process allows for multiblock brush formation, given the presence of active bromide chain-ends. To this point, diblock copolymer architectures with two electronically active blocks were fabricated, both with thicknesses controlled through irradiation time. As a proof of principle, poly(**M6MA**) was grown uniformly on ITO as the first block, followed by growth of patterned copolymers containing **M6MA** and **IrbtpMA** (10 mol

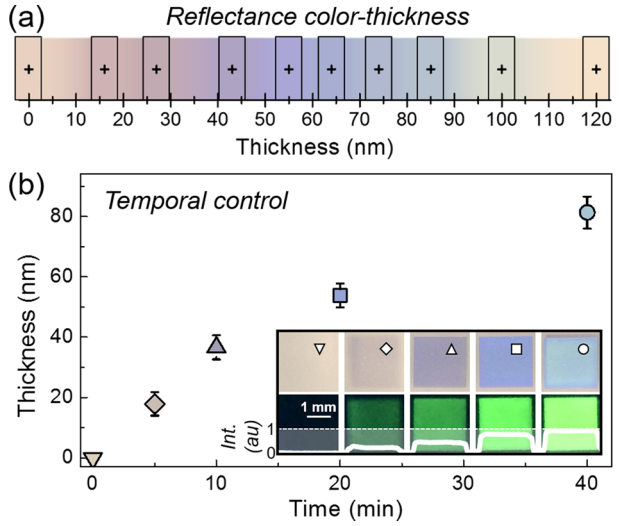

Figure 5. Temporal control over polymer brush growth on ITO. (a) Reflectance color-brush thickness correlation for poly(**M6MA**) determined using AFM and (b) growth of poly(**M6MA**-*co*-**IrppyMA**) over time, using 6 mol % **IrppyMA**. Inset shows reflectance (top) and photoluminescence (bottom, λ_{ex} = 365 nm) images, with normalized emission intensity as a cross-sectional average, demonstrating increased brightness with brush height.

%), to yield poly(**M6MA**-*b*-(**M6MA**-*co*-**IrbtpMA**)) brushes (Figure 6a). The chain extension is evident from photoluminescence spectroscopy, with the appearance of a red emission peak at ∼600 nm (Figure 6b). Additionally, reflectance microscopy shows two distinct colors for the first block,

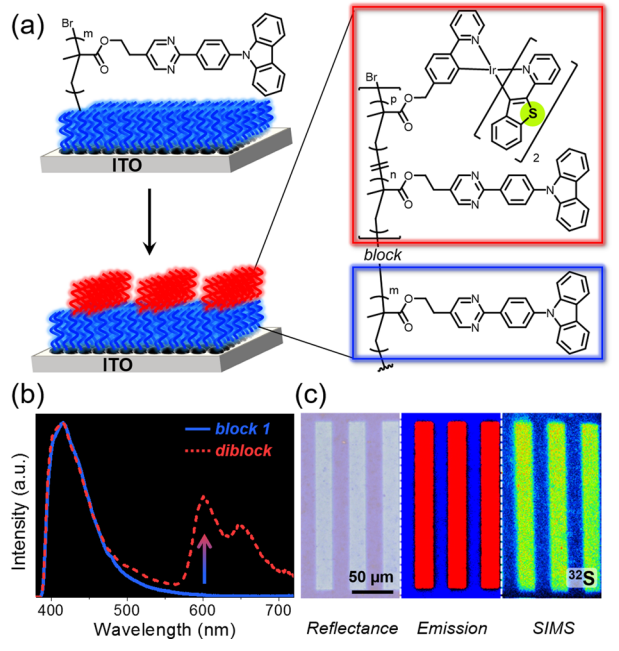

Figure 6. Diblock polymer brushes. (a) Schematic representation for diblock brush growth, and chemical structures for poly(**M6MA**), block 1, and poly(**M6MA**-*b*-(**M6MA**-*co*-**IrbtpMA**)), diblock. (b) Overlaid photoluminescence spectra before (blue solid line) and after (red dashed line) diblock brush growth. (c) Reflectance, emission, and SIMS images (from left to right) of the 20 × 200 μm^2 diblock copolymers. ^{32}S signal detected with SIMS, with increasing counts in going from blue to red.

DOI: 10.1021/acscentsci.7b00165
ACS Cent. Sci. 2017, 3, 654−661

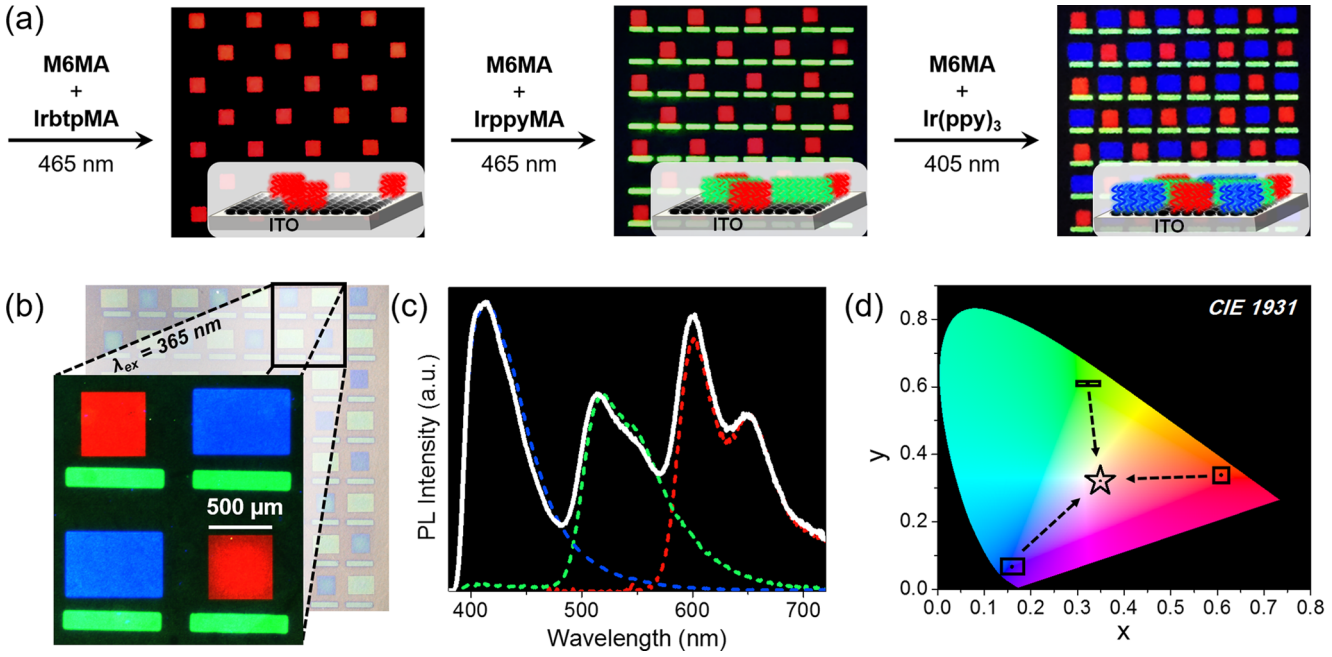

Figure 7. Generation of a red, green, and blue pixel array (PenTile RGBG format) on ITO through stepwise photopolymerizations using three different aligned photomasks. (a) Photoluminescence images (λ_{ex} = 365 nm) of the three step RGBG array fabrication, going from red (poly(**M6MA**-*co*-**IrbtpMA**); 500 × 500 μm^2), to green (poly(**M6MA**-*co*-**IrppyMA**); 125 × 750 μm^2), to blue (poly(**M6MA**); 500 × 750 μm^2) pixels. Schematic representations provided as insets. (b) Reflectance microscopy image and enlarged photoluminescence microscopy image (λ_{ex} = 365 nm) of the array. (c) Photoluminescence profile of the pixel array overlaid with individual RGB emission profiles. (d) CIE 1931 coordinates for the sum emission profile, (x, y) = (0.35, 0.32), shown as the white trace in "c" along with the individual red, (x, y) = (0.61, 0.34), green, (x, y) = (0.32, 0.61), and blue, (x, y) = (0.16, 0.07), coordinates.

poly(**M6MA**), and the diblock copolymer, correlating to a total thickness of ∼45 and 85 nm, respectively (Figure 6c). Photoluminescence microscopy indicates that the dopant resides solely in the 20 × 200 μm^2 rectangles (distinct red emission; Figure 6c), which was further confirmed with secondary ion mass spectrometry (SIMS), detecting the sulfur atoms (^{32}S) present in the **btp** ligand (Figure 6c). To demonstrate versatility, this procedure was also used to generate other diblock copolymer brushes (**M6MA**-*b*-(**M6MA**-*co*-**IrppyMA**)) (Figure S25).

The high degree of spatial control was further illustrated by the preparation of multicolored pixel arrays that are utilized in direct-lit display applications. The PenTile RGBG array of pixels used in active matrix OLEDs and plasma displays was chosen to showcase this methodology (Figure 7). Three chrome-coated glass photomasks were fabricated to contain different sized transparent rectangles for red, green, and blue pixels (masks 9–11, Figure S3), while a substrate holder composed of black Delrin and stainless still pins (Figure S2) was fabricated and used to align the masks. Sequentially, poly(**M6MA**-*co*-**IrbtpMA**), poly(**M6MA**-*co*-**IrppyMA**), and poly(**M6MA**) brushes were grown from ITO, providing red, green, and blue emissive rectangles, respectively (Figure 7a). Figure 7b shows a photoluminescence microscope image of the sample under 365 nm excitation, demonstrating well-defined features for the RGBG arrangement. The total photoluminescence output from the array was measured in an integrating sphere by exciting with UV light to determine the emission profile (Figure 7c) and chromaticity (Figure 7d).

Comparing the photoluminescence profiles for each individual pixel reveals good overlap with the sum "white" emission, demonstrating that it is simply a combination of the three different pixels, as would be the case in a direct-lit display. The chromaticity from the emission profile was generated following CIE guidelines, providing (x, y) coordinates of (0.35, 0.32), which is near the white point, as defined by illuminant DL65, (x, y) = (0.31, 0.33). Figure 7d also shows the individual CIE 1931 coordinates for red, green, and blue, which exhibits the underlying color mixing process that results in the "white" emission. The multicolored patterning clearly demonstrates that this new methodology is an effective way to fabricate pixel arrays from solution for OLED display applications.

As a final demonstration, monochromatic (Figure S27) and multicolored OLED devices were fabricated using the "grafting-from" procedure. Figure 8a provides a schematic representation of the multicolored device, with an architecture (from bottom up) of ITO/EML/HBL/ETL/EIL/Al, where ITO is the anode, polymer brushes comprise the EML, 5-(4-([1,1′-biphenyl]-3-yl)-6-phenyl-1,3,5-triazin-2-yl)-7,7-diphenyl-5,7-dihydroindeno-[2,1-*b*]carbazole acts as the HBL, 2,4-bis(9,9-dimethyl-9*H*-fluoren-2-yl)-6-(naphthalen-2-yl)-1,3,5-triazine comprises the

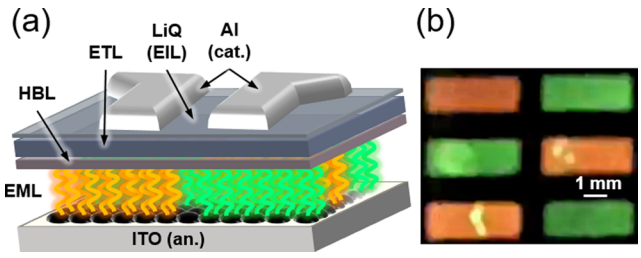

Figure 8. Multicolored OLED composed of poly(**M6MA**-*co*-**IrpqMA**) and poly(**M6MA**-*co*-**IrppyMA**) as the orange and green emitting regions, respectively. (a) Device architecture fabricated from the bottom up: ITO/EML/HBL/ETL/LiQ/Al. (b) Photograph showing electroluminescence of device under forward bias.

DOI: 10.1021/acscentsci.7b00165
ACS Cent. Sci. 2017, 3, 654–661

ETL, 8-hydroxy quinolinato lithium (LiQ), the electron injection layer (EIL), and aluminum (Al), the cathode. Two polymer brushes, poly(**M6MA**-*co*-**IrpqMA**), orange emitter, and poly(**M6MA**-*co*-**IrppyMA**), green emitter, were grafted from six ITO pixels on one glass substrate using low intensity visible irradiation through two chrome-coated glass photomasks (masks 16 and 17, Figure S3). Applying forward bias on a fully fabricated device prototype led to observable electroluminescence for all six pixels and two distinct colors (orange and green) as shown in Figure 8b. Current−voltage−light (JVL) device characterization was not performed owing to poor device lifetime/stability at voltages with observable light emission. Typically, the onset of light emission was observed between 8 and 9 V with images of pixel emission taken between 10 and 13 V. Short circuit formation was the primary failure mechanism between 8 and 13 V of potential. The high driving voltage is attributed to the lack of a hole injection layer, as well as a need for further material/device optimization. Significantly, turn-on of all six pixels suggests excellent brush coverage/uniformity with the potential of this platform for OLED display applications being clearly demonstrated by the ability to fabricate multicolored emissive devices.

CONCLUDING REMARKS

Electronically active and multicolored phosphorescent pixel arrays with remarkable control over size, shape, and architecture were demonstrated using a solution based approach. More specifically, low energy visible light could be used to graft patterned emissive polymer brushes from initiator functionalized ITO. Novel iridium monomers bearing a pendent methacrylate were synthesized and utilized for the dual purpose of catalyzing/mediating controlled radical polymerization and harnessing triplet energy through phosphorescence. The grafting of semiconducting methacrylate-based brushes using photoATRP provided emission spanning the visible spectrum, from blue to red, dictated by the C^N ligand (**X**) on the iridium complex. Moreover, the Ir(III) dopant content within the brushes was controlled by the monomer feed ratio, which allowed for white emission from RGB copolymer brushes. The facile fabrication of RGB pixel arrays for white emission and a working multicolored OLED prototype showcased the utility of this methodology for display applications. This novel platform opens up numerous multidisciplinary research opportunities, including the synthetic development of monomers for improved hole transport, the fabrication of functional nonlinear surfaces for improved light out-coupling, and pixel feature reduction for high resolution microdisplay applications.

ASSOCIATED CONTENT

Supporting Information

The Supporting Information is available free of charge on the ACS Publications website at DOI: 10.1021/acscentsci.7b00165.

Experimental details and further characterization (PDF)

AUTHOR INFORMATION

Corresponding Author

*E-mail: hawker@mrl.ucsb.edu.

ORCID

Craig J. Hawker: 0000-0001-9951-851X

Notes

The authors declare no competing financial interest.

ACKNOWLEDGMENTS

We thank the MRSEC program of the National Science Foundation (DMR 1121053) and The Dow Chemical Company through the Dow Materials Institute at UCSB for financial support. The authors acknowledge the use of the Microfluidics Laboratory and NCF Cleanroom within the California Nano-Systems Institute. We thank Dr. David Bothman for help with photomask and substrate holder design and Dr. David Devore (Dow) for insightful discussions. C.W.P. acknowledges the Alexander von Humboldt foundation for financial support.

REFERENCES

(1) Gao, H.-Y.; Yao, Q.-X.; Liu, P.; Zheng, Z.-Q.; Liu, J.-C.; Zheng, H.-D.; Zeng, C.; Yu, Y.-J.; Sun, T.; Zeng, Z.-X. Latest Development of Display Technologies. *Chin. Phys. B* **2016**, *25* (9), 094203.

(2) OLED Microdisplays: Technology and Applications. In *OLED Microdisplays: Technology and Applications*; Templier, F., Ed.; Wiley-ISTE, 2014; pp 231−246.

(3) Diao, Y.; Shaw, L.; Bao, Z.; Mannsfeld, S. C. B. Morphology Control Strategies for Solution-Processed Organic Semiconductor Thin Films. *Energy Environ. Sci.* **2014**, *7*, 2145−2159.

(4) Ho, S.; Liu, S.; Chen, Y.; So, F. Review of Recent Progress in Multilayer Solution-Processed Organic Light-Emitting Diodes. *J. Photonics Energy* **2015**, *5* (1), 057611.

(5) Wu, Z.; Ma, D. Recent Advances in White Organic Light-Emitting Diodes. *Mater. Sci. Eng., R* **2016**, *107*, 1−42.

(6) Gather, M. C.; Köhnen, A.; Meerholz, K. White Organic Light-Emitting Diodes. *Adv. Mater.* **2011**, *23* (2), 233−248.

(7) D'Andrade, B. W.; Forrest, S. R. White Organic Light-Emitting Devices for Solid-State Lighting. *Adv. Mater.* **2004**, *16* (18), 1585−1595.

(8) Wu, S.; Li, S.; Sun, Q.; Huang, C.; Fung, M.-K. Highly Efficient White Organic Light-Emitting Diodes with Ultrathin Emissive Layers and a Spacer-Free Structure. *Sci. Rep.* **2016**, *6*, 25821.

(9) Kim, J. W.; You, S.; Kim, N. H.; Yoon, J.-A.; Cheah, K. W.; Zhu, F. R.; Kim, W. Y. Study of Sequential Dexter Energy Transfer in High Efficient Phosphorescent White Organic Light-Emitting Diodes with Single Emissive Layer. *Sci. Rep.* **2015**, *4*, 7009.

(10) Reineke, S.; Lindner, F.; Schwartz, G.; Seidler, N.; Walzer, K.; Lüssem, B.; Leo, K. White Organic Light-Emitting Diodes with Fluorescent Tube Efficiency. *Nature* **2009**, *459* (7244), 234−238.

(11) Pardo, D. A.; Jabbour, G. E.; Peyghambarian, N. Application of Screen Printing in the Fabrication of Organic Light-Emitting Devices. *Adv. Mater.* **2000**, *12* (17), 1249−1252.

(12) Choi, J.; Kim, D.; Yoo, P. J.; Lee, H. H. Simple Detachment Patterning of Organic Layers and Its Application to Organic Light-Emitting Diodes. *Adv. Mater.* **2005**, *17* (2), 166−171.

(13) Oh, S.; Park, S. K.; Kim, J. H.; Cho, I.; Kim, H.; Park, S. Y. Patterned Taping: A High-Efficiency Soft Lithographic Method for Universal Thin Film Patterning. *ACS Nano* **2016**, *10*, 3478−3485.

(14) Jung, S.-H.; Kim, J.-J.; Kim, H.-J. High Performance Inkjet Printed Phosphorescent Organic Light Emitting Diodes Based on Small Molecules Commonly Used in Vacuum Processes. *Thin Solid Films* **2012**, *520* (23), 6954−6958.

(15) Muller, C. D.; Falcou, A.; Reckefuss, N.; Rojahn, M.; Wiederhirn, V.; Rudati, P.; Frohne, H.; Nuyken, O.; Becker, H.; Meerholz, K. Multi-Colour Organic Light-Emitting Displays by Solution Processing. *Nature* **2003**, *421*, 829−833.

(16) Scheler, E.; Strohriegl, P. Three Color Random Fluorene-Based Oligomers for Fast Micrometer-Scale Photopatterning. *Chem. Mater.* **2010**, *22*, 1410−1419.

(17) Gather, B. M. C.; Köhnen, A.; Falcou, A.; Becker, H.; Meerholz, K. Solution-Processed Full-Color Polymer Organic Light-Emitting Diode Displays Fabricated by Direct Photolithography. *Adv. Funct. Mater.* **2007**, *17*, 191−200.

(18) Ventsch, F.; Gather, M. C.; Meerholz, K. Towards Organic Light-Emitting Diode Microdisplays with Sub-Pixel Patterning. *Org. Electron.* **2010**, *11*, 57−61.

DOI: 10.1021/acscentsci.7b00165
ACS Cent. Sci. 2017, 3, 654−661

(19) Derue, L.; Olivier, S.; Tondelier, D.; Maindron, T.; Geffroy, B.; Ishow, E. All-Solution-Processed Organic Light-Emitting Diodes Based on Photostable Photo-Cross-Linkable Fluorescent Small Molecules. *ACS Appl. Mater. Interfaces* **2016**, *8*, 16207−16217.
(20) Doubina, N.; Jenkins, J. L.; Paniagua, S. A.; Mazzio, K. A.; MacDonald, G. A.; Jen, A. K. Y.; Armstrong, N. R.; Marder, S. R.; Luscombe, C. K. Surface-Initiated Synthesis of poly(3-Methylthiophene) from Indium Tin Oxide and Its Electrochemical Properties. *Langmuir* **2012**, *28* (3), 1900−1908.
(21) Huddleston, N. E.; Sontag, S. K.; Bilbrey, J. A.; Sheppard, G. R.; Locklin, J. Palladium-Mediated Surface-Initiated Kumada Catalyst Polycondensation: A Facile Route towards Oriented Conjugated Polymers. *Macromol. Rapid Commun.* **2012**, *33* (24), 2115−2120.
(22) Beryozkina, T.; Boyko, K.; Khanduyeva, N.; Senkovskyy, V.; Horecha, M.; Oertel, U.; Simon, F.; Stamm, M.; Kiriy, A. Grafting of Polyfluorene by Surface-Initiated Suzuki Polycondensation. *Angew. Chem., Int. Ed.* **2009**, *48* (15), 2695−2698.
(23) Snaith, H. J.; Whiting, G. L.; Sun, B.; Greenham, N. C.; Huck, W. T. S.; Friend, R. H. Self-Organization of Nanocrystals in Polymer Brushes. Application in Heterojunction Photovoltaic Diodes. *Nano Lett.* **2005**, *5* (9), 1653−1657.
(24) Yan, J.; Pan, X.; Schmitt, M.; Wang, Z.; Bockstaller, M. R.; Matyjaszewski, K. Enhancing Initiation Efficiency in Metal-Free Surface-Initiated Atom Transfer Radical Polymerization (SI-ATRP). *ACS Macro Lett.* **2016**, *5* (6), 661−665.
(25) Narupai, B.; Poelma, J. E.; Pester, C. W.; McGrath, A. J.; Toumayan, E. P.; Luo, Y.; Kramer, J. W.; Clark, P. G.; Ray, P. C.; Hawker, C. J. Hierarchical Comb Brush Architectures via Sequential Light-Mediated Controlled Radical Polymerizations. *J. Polym. Sci., Part A: Polym. Chem.* **2016**, *54* (15), 2276−2284.
(26) Pester, C. W.; Narupai, B.; Mattson, K. M.; Bothman, D. P.; Klinger, D.; Lee, K. W.; Discekici, E. H.; Hawker, C. J. Engineering Surfaces through Sequential Stop-Flow Photopatterning. *Adv. Mater.* **2016**, *28*, 9292−9300.
(27) Discekici, E. H.; Pester, C. W.; Treat, N. J.; Lawrence, J.; Mattson, K. M.; Narupai, B.; Toumayan, E. P.; Luo, Y.; McGrath, A. J.; Clark, P. G.; Read De Alaniz, J.; Hawker, C. J. Simple Benchtop Approach to Polymer Brush Nanostructures Using Visible-Light-Mediated Metal-Free Atom Transfer Radical Polymerization. *ACS Macro Lett.* **2016**, *5* (2), 258−262.
(28) Li, B.; Yu, B.; Ye, Q.; Zhou, F. Tapping the Potential of Polymer Brushes through Synthesis. *Acc. Chem. Res.* **2015**, *48* (2), 229−237.
(29) Poelma, J. E.; Fors, B. P.; Meyers, G. F.; Kramer, J. W.; Hawker, C. J. Fabrication of Complex Three-Dimensional Polymer Brush Nanostructures through Light-Mediated Living Radical Polymerization. *Angew. Chem., Int. Ed.* **2013**, *52* (27), 6844−6848.
(30) Leibfarth, F. A.; Mattson, K. M.; Fors, B. P.; Collins, H. A.; Hawker, C. J. External Regulation of Controlled Polymerizations. *Angew. Chem., Int. Ed.* **2013**, *52*, 199−210.
(31) Li, B.; Yu, B.; Huck, W. T. S.; Liu, W.; Zhou, F. Electrochemically Mediated Atom Transfer Radical Polymerization on Nonconducting Substrates: Controlled Brush Growth through Catalyst Diffusion. *J. Am. Chem. Soc.* **2013**, *135*, 1708−1710.
(32) Fors, B. P.; Hawker, C. J. Control of a Living Radical Polymerization of Methacrylates by Light. *Angew. Chem., Int. Ed.* **2012**, *51* (35), 8850−8853.
(33) Lamansky, S.; Djurovich, P.; Murphy, D.; Abdel-Razzaq, F.; Lee, H. E.; Adachi, C.; Burrows, P. E.; Forrest, S. R.; Thompson, M. E. Highly Phosphorescent Bis-Cyclometalated Iridium Complexes: Synthesis, Photophysical Characterization, and Use in Organic Light Emitting Diodes. *J. Am. Chem. Soc.* **2001**, *123* (18), 4304−4312.
(34) Ulbricht, C.; Beyer, B.; Friebe, C.; Winter, A.; Schubert, U. S. Recent Developments in the Application of Phosphorescent iridium-(III) Complex Systems. *Adv. Mater.* **2009**, *21*, 4418−4441.
(35) Deng, Y.-L.; Cui, L.-S.; Liu, Y.; Wang, Z.-K.; Jiang, Z.-Q.; Liao, L.-S. Solution-Processable Iridium Phosphors for Efficient Red and White Organic Light-Emitting Diodes with Low Roll-Off. *J. Mater. Chem. C* **2016**, *4*, 1250−1256.
(36) Sudhakar, M.; Djurovich, P. I.; Hogen-Esch, T. E.; Thompson, M. E. Phosphorescence Quenching by Conjugated Polymers. *J. Am. Chem. Soc.* **2003**, *125*, 7796−7797.
(37) Sandee, A. J.; Williams, C. K.; Evans, N. R.; Davies, J. E.; Boothby, C. E.; Kohler, A.; Friend, R. H.; Holmes, A. B. Solution-Processible Conjugated Electrophosphorescent Polymers. *J. Am. Chem. Soc.* **2004**, *126*, 7041−7048.
(38) Poulsen, B. D. A.; Kim, B. J.; Ma, B.; Zonte, C. S.; Frechet, J. M. J. Site Isolation in Phosphorescent Bichromophoric Block Copolymers Designed for White Electroluminescence. *Adv. Mater.* **2010**, *22*, 77−82.
(39) Page, Z. A.; Chiu, C.-Y.; Narupai, B.; Laitar, D. S.; Mukhopadhyay, S.; Sokolov, A.; Hudson, Z. M.; Bou Zerdan, R.; McGrath, A. J.; Kramer, J. W.; Barton, B. E.; Hawker, C. J. Highly Photoluminescent Nonconjugated Polymers for Single-Layer Light Emitting Diodes. *ACS Photonics* **2017**, *4*, 631−641.
(40) Nonoyama, M. Benzo[h]quinolin-10-Yl-N Iridium(III) Complexes. *Bull. Chem. Soc. Jpn.* **1974**, *47*, 767−768.
(41) Pujari, S. P.; Scheres, L.; Marcelis, A. T. M.; Zuilhof, H. Covalent Surface Modification of Oxide Surfaces. *Angew. Chem., Int. Ed.* **2014**, *53* (25), 6322−6356.
(42) Li, Y.; Giesbers, M.; Gerth, M.; Zuilhof, H. Generic Top-Functionalization of Patterned Antifouling Zwitterionic Polymers on Indium Tin Oxide. *Langmuir* **2012**, *28* (34), 12509−12517.
(43) Li, Y.; Zuilhof, H. Photochemical Grafting and Patterning of Organic Monolayers on Indium Tin Oxide Substrates. *Langmuir* **2012**, *28* (12), 5350−5359.
(44) Huang, C.; Tassone, T.; Woodberry, K.; Sunday, D.; Green, D. L. Impact of ATRP Initiator Spacer Length on Grafting Poly(methyl Methacrylate) from Silica Nanoparticles. *Langmuir* **2009**, *25*, 13351−13360.
(45) Dolinski, N. D.; Page, Z. A.; Eisenreich, F.; Niu, J.; Hecht, S.; Read de Alaniz, J.; Hawker, C. J. A Versatile Approach for In Situ Monitoring of Photoswitches and Photopolymerizations. *ChemPhotoChem.* **2017**, *1*, 125−131.
(46) Chung, Y.; Murmann, B.; Selvarasah, S.; Dokmeci, M. R.; Bao, Z. Low-Voltage and Short-Channel Pentacene Field-Effect Transistors with Top-Contact Geometry Using Parylene-C Shadow Masks. *Appl. Phys. Lett.* **2010**, *96*, 133306.
(47) Ji, Y.; Ran, F.; Xu, H.; Shen, W.; Zhang, J. Improved Performance and Low Cost OLED Microdisplay with Titanium Nitride Anode. *Org. Electron.* **2014**, *15* (11), 3137−3143.
(48) Xie, G.; Xue, Q.; Chen, P.; Tao, C.; Zhao, C.; Lu, J.; Gong, Z.; Zhang, T.; Huang, R.; Du, H.; Xie, W.; Hou, J.; Zhao, Y.; Liu, S. Highly Efficient and Low-Cost Top-Emitting Organic Light-Emitting Diodes for Monochromatic Microdisplays. *Org. Electron.* **2010**, *11* (3), 407−411.
(49) Can, C.; Underwood, I. Compact and Efficient RGB to RGBW Data Conversion Method and Its Application in OLED Microdisplays. *J. Soc. Inf. Disp.* **2013**, *21* (3), 109−119.

DOI: 10.1021/acscentsci.7b00165
ACS Cent. Sci. 2017, 3, 654−661